Chemical Science

ROYAL SOCIETY OF CHEMISTRY

EDGE ARTICLE

View Article Online
View Journal | View Issue

Cite this: *Chem. Sci.*, 2021, **12**, 12391

All publication charges for this article have been paid for by the Royal Society of Chemistry

Tuning of bandgaps and emission properties of light-emitting diode materials through homogeneous alloying in molecular crystals†

Reshmi Thomas, §[a] Sajesh P. Thomas, ‡§[a] Harish Lakhotiya, [a] Aref H. Mamakhel, [a] Martin Bondesgaard, [a] Victoria Birkedal [b] and Bo B. Iversen *[a]

Received 8th July 2021
Accepted 14th August 2021

DOI: 10.1039/d1sc03714e

rsc.li/chemical-science

Alloy formation is ubiquitous in inorganic materials science, and it strongly depends on the similarity between the alloyed atoms. Since molecules have widely different shapes, sizes and bonding properties, it is highly challenging to make alloyed molecular crystals. Here we report the generation of homogenous molecular alloys of organic light emitting diode materials that leads to tuning in their bandgaps and fluorescence emission. Tris(8-hydroxyquinolinato)aluminium (Alq_3) and its Ga, In and Cr analogues (Gaq_3, Inq_3, and Crq_3) form homogeneous mixed crystal phases thereby resulting in binary, ternary and even quaternary molecular alloys. The $M_xM'_{(1-x)}q_3$ alloy crystals are investigated using X-ray diffraction, energy dispersive X-ray spectroscopy and Raman spectroscopy on single crystal samples, and photoluminescence properties are measured on the exact same single crystal specimens. The different series of alloys exhibit distinct trends in their optical bandgaps compared with their parent crystals. In the $Al_xGa_{(1-x)}q_3$ alloys the emission wavelengths lie in between those of the parent crystals, while the $Al_xIn_{(1-x)}q_3$ and $Ga_xIn_{(1-x)}q_3$ alloys have red shifts. Intriguingly, efficient fluorescence quenching is observed for the $M_xCr_{(1-x)}q_3$ alloys (M = Al, Ga) revealing the effect of paramagnetic molecular doping, and corroborating the molecular scale phase homogeneity.

Introduction

Alloy formation represents one of the cornerstones in inorganic materials science. Ever since the bronze age, humankind has relied on numerous materials that owe their unique properties to the continuous mixing of similar atoms or ions in the crystalline state thereby forming solids with random disorder. In sharp contrast the formation of alloys between molecular species is highly challenging since molecules are unique in size, shape and properties. Crystal engineering approaches directed towards multi-component crystals are largely based on cocrystal design utilizing supramolecular synthons that non-covalently bind different component molecules in crystals.[1] While cocrystals are limited to the fixed stoichiometries of molecular components, organic alloys are characterized by their continuous stoichiometries in crystals. Since the possibilities of different molecular components occupying similar crystal lattices are limited, the reports of molecular alloy crystals are relatively rare.[2–10] Moreover, studies that explore tuning of physical properties of molecular materials by alloy formation are even rarer – despite the promising prospects of alloys in bandgap engineering of organic semiconductors and molecular photovoltaic crystals.[11,12] Although mixed solid state phases formed by melt-cooling of different molecular components, or by doping in polymer matrices, are sometimes referred to as alloy phases, these composite phases need to be clearly distinguished from molecular alloy crystals, which are strictly characterized by homogenous mixing of molecular components in their crystal lattices. Studies of metal organic frameworks and organic–inorganic hybrid perovskite structures that show composition variation with respect to ionic species in the crystal lattices have been reported with tuning in the optical/electrical properties, but they are not strictly classified as organic alloys.[13,14] A well-known class of organic alloy crystals are those formed by donor–acceptor charge transfer complexes. Matzger *et al.* and Pei *et al.* explored the variation in bandgaps of molecular solid solutions, but continuous or systematic trends in bandgaps could not be observed in these alloys.[15,16] Recently, we demonstrated systematic tuning in the optical band gaps in molecular alloys formed by a series of diphenyl

[a]*Center for Materials Crystallography, Department of Chemistry and iNano, Aarhus University, Langelandsgade 140, Aarhus 8000, Denmark. E-mail: bo@chem.au.dk*

[b]*Interdisciplinary Nanoscience Centre (iNano) and Department of Chemistry, Aarhus University, Langelandsgade 140, Aarhus 8000, Denmark*

† Electronic supplementary information (ESI) available. See DOI: 10.1039/d1sc03714e

§ These authors contributed equally.

‡ Current address: Department of Chemistry, Indian Institute of Technology Delhi, New Delhi-110016, India.

dichalcogenides.[17] In the context of photophysical properties of molecular alloys, Fu *et al.* demonstrated the tuning of photoluminescence emission and optical waveguiding performances of charge transfer alloy crystals formed by perylene and 9,10-dicyano-anthracene $(DCA)_{1-x}(Pe)_x$.[18] Although the composition range of the alloy components in these examples were limited to <10%, this report points to the prospects of achieving desirable tuning of photophysical properties if high composition ranges could be achieved in molecular alloys. In this article, we report the crystalline molecular alloys formed by organic light-emitting diode (OLED) materials Mq_3, where M = Al, Ga, In, and Cr and q = 8-hydroxyquinoline ligand. Tris(8-hydroxyquinoline)aluminum or Alq_3 is widely used as the light emitting layer material in OLED devices.[19,20] Light emission is generated in such emissive layers by electron–hole recombination. Hence, it is logical to assume that the tuning of bandgaps (such as the trend reported by us in dichalcogenide molecular alloys[17]) may also result in the tuning of emission properties of OLED components such as Alq_3. Tuning of emission properties in Mq_3 compounds are primarily attempted by means of chemical derivatives of the ligand molecule by adding functional groups to 8-hydroxyquinoline ligand.[21,22] However, such methods result in significant changes from the original crystal structure of Mq_3 in packing features, intermolecular interactions and thereby in opto-electronic properties. Recently, Han *et al.* reported alloy crystal forms of Mq_3 methanol solvates and Mq_3 nano/microrods obtained through a solution pathway.[23] However, the structural characterization of the mixed crystals were limited to the solvate crystal $Al_{0.5}Ga_{0.5}q_3$·MeOH, the crystal structure of which was quite different from that of the pure Alq_3 or Gaq_3. To our knowledge there is no systematic structure–property relation study on the multicomponent molecular alloy forms of Mq_3 series of crystalline OLED materials. Here we report the binary, tertiary and quaternary molecular alloys of Alq_3, Gaq_3, Inq_3, and Crq_3 that form homogenously mixed crystal phases. A detailed structural study correlating the crystal structures, composition and domain structures with the trends in optical band gaps and fluorescence emission properties observed for the alloy crystals is described here employing single crystal X-ray diffraction (SCXRD), powder XRD, energy dispersive X-ray (EDX), Raman and fluorescence spectroscopy. Since Mq_3 systems exhibit multiple crystal polymorphs and two different stereoisomers (see Fig. 1a), the effect of such structural preferences in the alloy formation and emission properties are investigated. In addition, we report an hitherto unknown phenomenon of fluorescence quenching in molecular alloys (in the alloy crystals formed by Crq_3) revealing the effect of paramagnetic molecular doping/impurity on the emission properties of these OLED materials.

Results and discussion

Polymorphs and stereoisomers of Mq_3 compounds and the generation of their alloy crystals

In this study, we employed a two-zone sublimation–condensation method to obtain crystals of the Mq_3 compounds. The Mq_3 series of compounds exhibit two stereoisomers; a meridional (*mer*) isomer with C_1 symmetry and facial (*fac*) isomer with C_3 symmetry, as shown in Fig. 1a. They are known to crystallize in five different crystal forms – resulting from a combination of polymorphs and stereoisomers – referred to as α, β, γ, δ, and ε. While α, β, and ε forms are adopted by the *mer* isomer, the γ and δ forms are associated with the *fac* stereoisomer.[24,25] The central metal atom M is in +3 oxidation state in all the Mq_3 compounds discussed here. The preferences for the stereoisomers are known to be different in the series of Mq_3 compounds, depending upon the size and covalent radii of the central metal atom. The preference for *fac* or *mer* isomer is a result of the tradeoff between two opposite factors[26] (i) the structure destabilizing steric effect between the ligands which is higher in *fac* form and increases with decreasing covalent radii, (ii) the stabilizing effect from stronger metal–ligand orbital interactions and bonding, which is predominant in the *fac* isomer. It is also known that the In–N and In–O bonds are more covalent as compared to other M–O and M–N bonds in this series.[20] Hence, for Alq_3, Gaq_3, and Crq_3 the *mer* isomer is found to be more stable, whereas for Inq_3 the *fac* isomer is preferred (owing to the higher covalent radius of In). The crystal forms obtained in this study are in accordance with this trend in stability of isomers.

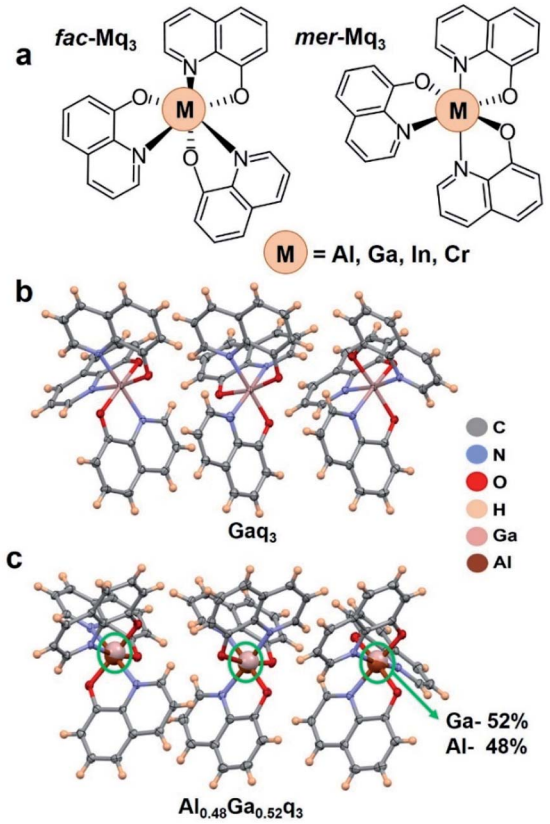

Fig. 1 (a) The two possible stereoisomers, namely meridional (*mer*) and facial (*fac*), of Mq_3 molecules discussed in this study, where M = Al, Ga, In, and Cr and q = 8-hydroxyquinoline ligand. Asymmetric units of (b) the new polymorph of Gaq_3 and (c) the binary alloy $Al_{0.48}Ga_{0.52}q_3$ shown as thermal ellipsoid plots at the 50% probability level (metal atoms of the alloy structure have been highlighted as enlarged balls).

For Alq_3, Gaq_3 and Crq_3 the crystal forms obtained by two-zone sublimation–condensation method were determined to be *mer*-ε form, whereas the Inq_3 crystals obtained were found to be predominantly *fac*-δ form. The crystals showed acicular morphology (Fig. S1†), and their crystal structures were confirmed by single crystal XRD experiments at 100 K, except for Inq_3 for which the poor quality of the single crystals allowed only the determination of unit cell parameters. Table S2 in the ESI† shows the crystallographic cell parameters for the different crystal forms discussed here. The crystal structures of *mer*-ε form adopted by Alq_3 and Crq_3 have $Z = 6$, with 3 molecules in the asymmetric unit ($Z' = 3$) and crystallographic space group $P\bar{1}$. The cell parameters of Alq_3 and Crq_3 showed similarity implying their isostructurality. Although only the β form of Gaq_3 is known (CSD code: ETELAQ), in this study we discovered a new polymorph of Gaq_3 $Z = 6$ and $Z' = 3$ in triclinic space group $P\bar{1}$, which is isostructural to the ε form of Alq_3 and Crq_3. Fig. S2 in the ESI† shows the crystal packing diagrams of *mer*-Gaq_3 in β and ε forms. The discovery of this *mer*-ε polymorph points to the propensity of Gaq_3 to potentially occupy the lattice of Alq_3 or Crq_3 crystals.

A commonly reported class of solid solution/alloy crystals are formed between planar aromatic molecules as donor–acceptor charge transfer complexes, where two or more electron-acceptor molecules are sandwiched between planar aromatic electron donor molecules.[15,18,27] Hence the individual crystal structures of the electron-acceptor molecules are not a crucial factor in the alloy formation. On the contrary, for nonplanar molecules to form alloys, isostructurality of the crystal structures of individual components is an important structural criterion.

The crystal structures of the Mq_3 compounds (Alq_3, Gaq_3, Crq_3 and Inq_3) are stabilized by intermolecular C–H$\cdots\pi$, C–H$\cdots$O interactions and $\pi\cdots\pi$ stacking interactions (with a partial stacking of the aromatic rings). To obtain a more quantitative understanding of the crystal packing and interactions in these structures, we employed Hirshfeld fingerprint analysis[28] which revealed percentage contribution of different types of intermolecular contacts. Hirshfeld surface analysis revealed that the isostructurality in crystal packing and unit cell parameters also manifest as the percentage contributions of C$\cdots$C and H$\cdots$C, and H$\cdots$O interatomic contacts (corresponding to the proportions of C–H… π, C–H$\cdots$O interactions and $\pi\cdots\pi$ stacking interactions) – which are very similar among the series of Mq_3 crystal structures (Fig. S3 and Table S1†). These results are akin to the previously reported examples of isostructural interaction topologies in analogous crystal structures[4,17] reported by us (represented as energy frameworks[29]), which facilitated alloy formation. Their unit cell volumes are also very similar, and show the following order: $V_{cell}(Alq_3) < V_{cell}(Gaq_3) < V_{cell}(Crq_3)$ (see ESI Table S2†).

Inspired by the isostructurality of Alq_3, Gaq_3 and Crq_3 (as can be seen from Tables S1 and S2†), we further probed the possibility of alloy formation between these compounds. It should be noted that Han *et al.* recently reported mixed alloy-like crystals of Mq_3 solvates and crystalline nanorods.[23] The powder diffractograms of the nano/microrods obtained by the mixed phases of Alq_3 and Gaq_3 from chloroform solvent indicated a possible α polymorph formation, although these phases were not structurally characterized. Moreover, the composition of the alloy phases were not determined but arbitrarily assigned to the ratio of parent compounds used for crystallization. Here, firstly we set out to synthesize binary molecular alloys using the following combinations: Alq_3–Gaq_3, Alq_3–Crq_3 and Gaq_3–Crq_3 in different stoichiometric ratios. In order to obtain the single crystals of the binary alloys devoid of any solvent molecules (that might potentially co-crystallize and alter the crystal structure), we employed two-zone sublimation–condensation method. Crystals of Alq_3–Gaq_3, Alq_3–Crq_3 and Gaq_3–Crq_3 alloy phases thus obtained were of acicular morphology, very similar to their parent crystals. SCXRD analysis of the single crystals of the alloys revealed a wide range of compositions (see Tables S3–S7†). We have recently demonstrated that single crystals of molecular alloys obtained from the same crystallization experiment can show a range of composition of their components.[17] Here, we find that accurate stoichiometry control in the alloy crystals is not possible for the systems in this study (using the sublimation–condensation method). Nevertheless, the compositions of the alloy single crystals from SCXRD roughly match with the stoichiometry of the compound mixtures used in their crystallization although with some exceptions (see Tables S3–S7†). The deviation of the composition from their starting stoichiometries were particularly dominant for the alloy crystals containing Crq_3, where the percentage of Crq_3 was generally found to be higher than the stoichiometry used in the crystallization mixture.

As opposed to Alq_3, Gaq_3 and Crq_3, the readily obtained form of Inq_3 is the *fac* isomer crystallizing in δ form ($Z = 2$). Although the *mer*-Inq_3 is reported, it crystallizes in β form (CSD code: WADGUZ).[30] Hence, the alloys of Inq_3 with other Mq_3 compounds were found to be quite difficult to obtain possibly due to the fact that Inq_3 prefers a *fac* stereoisomer as opposed to the other three Mq_3 compounds. We could not obtain alloy single crystals of Inq_3 with Alq_3, Gaq_3 or Crq_3 for higher composition of Inq_3 in the alloy form. Since the major focus of this study is to obtain structure–property relations in the molecular alloys of this series of OLED materials at a molecular to crystal domain level, our investigations were focused mainly on single crystals. Because good quality single crystals could not be obtained for 30% and 50% alloys of Inq_3 with Alq_3 and Gaq_3, we used powder-XRD to characterize these phases (see ESI†). Molecular alloy formation inherently leads to crystallographic disorders with respect to both positions and site occupancy values, and we tested two strategies to model the alloy crystal structures. The structural models with constraints on the positions and atomic displacement parameters (ADPs) of the central metal atoms of Mq_3 were especially found to result in satisfactory convergence in the crystallographic refinements. The occupancy values of metal atoms in the binary alloy crystals were refined using an occupancy free variable (see ESI†).

It is interesting to note some structural features of Mq_3 compounds that exhibit changes in the alloy crystal structures as compared to their parent crystal forms. The metal–ligand bond distances (M–O and M–N bonds) in the series of Mq_3 structures and in the alloys are of particular interest. The average M–O distances for the series of Mq_3 crystal structures from the SCXRD

analysis are in the following order: Alq_3 (1.86 Å) < Gaq_3 (1.95 Å) < Crq_3 (1.96 Å). Whereas the M–N bond distances shows the order of Alq_3 (2.03 Å) < Crq_3 (2.04 Å) < Gaq_3 (2.08 Å). Interestingly, the M–O and M–N bond distances in the alloy crystal structures are found to be intermediate between the corresponding bond distances in their parent crystal structures. Fig. 2 shows the trends in M–O and M–N bond distances in Alq_3–Gaq_3 and Alq_3–Crq_3 alloy crystals, with the bond distance variations roughly corelating with the composition of the alloys (also, see Table S9†). This 'bond averaging effect' in the alloy crystals is likely due to the spatial averaging of the corresponding metal and ligand atom positions in the alloy crystals, rather than a realistic bond elongation/compression of the M–O and M–N bonds. However, this indicates the ability of different component Mq_3 molecules to occupy very similar crystallographic positions in the alloy crystal lattice in a more or less homogenous manner.

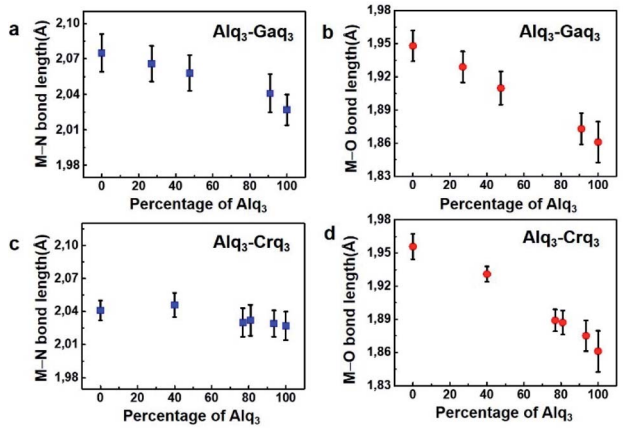

Fig. 2 Variations in M–O and M–N bond distances observed in the crystal structures of (a, b) Alq_3–Gaq_3 and (c, d) Alq_3–Crq_3 alloys with respect to the corresponding bond distances in their parent crystal structures.

Ternary and quaternary alloy crystals of Mq_3

Further, we set out to examine if ternary and quaternary molecular alloys could be obtained from this series of Mq_3 compounds. By extending the same crystallization approach with 1 : 1 : 1 stoichiometric ratio of Alq_3, Gaq_3 and Crq_3 as well as 1 : 1 : 1 : 1 mixture of Alq_3, Crq_3, Gaq_3 and Inq_3, we obtained single crystals which were further analyzed using SCXRD and EDX spectroscopy. For binary molecular alloys, the composition obtained from EDX spectra were found to be comparable to the values obtained from SCXRD. However, for ternary and quaternary alloy crystals, the crystallographic occupancy refinement of the closely positioned metal atoms into three or four linearly correlated free variable failed to attain convergence (leading to unreasonable values of occupancies, including negative occupancies). Hence, to obtain realistic crystal structure models for the three component and four component alloys, we measured EDX spectra on the same single crystals used for SCXRD data collection (Fig. 3a and b). The crystal structures of the ternary and quaternary alloys are thus refined using SCXRD data with values of metal atom occupancies fixed to the composition values obtained from the EDX spectra. To our knowledge, these structures represent the rare examples of quaternary molecular alloys (medium entropy alloys) formed by nonplanar molecules. The examples of six-component solid-solutions with three stoichiometry-tunable molecular components reported by Desiraju *et al.*,[7,8] and the quaternary solid solutions of donor–acceptor type charge transfer complexes reported by Matzger *et al.* are to be noted in this context.[15]

Spectroscopic studies of the domain structure and homogeneity of the alloy crystals

Although SCXRD provides the structure of the alloy crystals with multiple components in the lattice, it gives only a spatially averaged picture of the molecules in the alloy crystals. Beyond molecular structure and crystallographic parameters, domain structure is an important feature in alloy crystal phases that influences their physical properties. The long-range

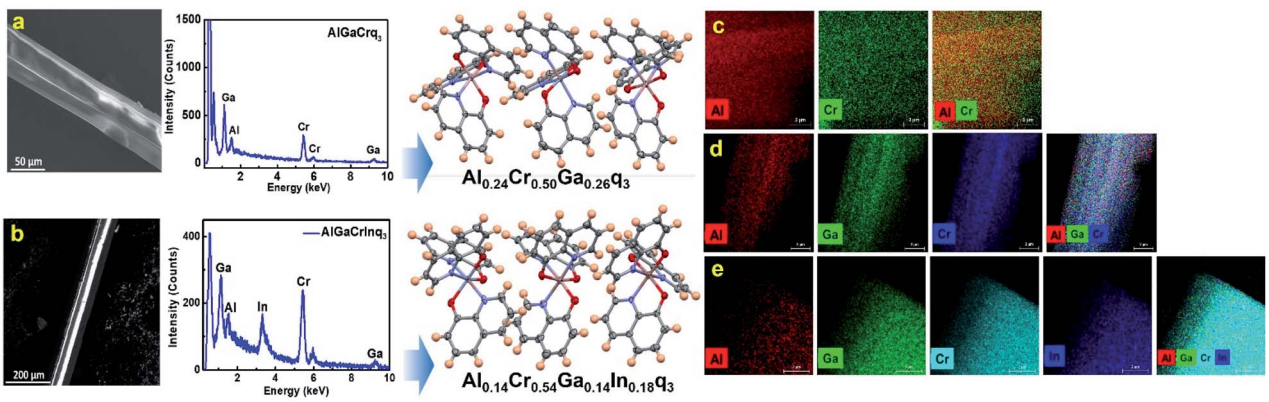

Fig. 3 Scanning electron microscopic images of (a) ternary and (b) quaternary alloy single crystals along with their EDX spectra, and the corresponding single crystal X-ray structural models (thermal ellipsoid plot at 50% probability level) obtained using the composition values from the EDX spectra. EDX maps of alloy crystals showing the homogenous distribution of their components in (c) Alq_3–Crq_3 binary, (d) Alq_3–Gaq_3–Crq_3 ternary and (e) Alq_3–Gaq_3–Inq_3–Crq_3 quaternary alloys.

distribution of molecular components in a homogenous or heterogenous manner can dictate the degree of mixing of electronic states corresponding to individual components in the alloy crystals. In a recent report, we investigated the molecular alloy crystals formed by diphenyl disulfide and diphenyl diselenide analogues using EDX spectroscopy revealing a homogenous distribution in the alloy phases.[17] In this study, we employed EDX spectroscopy to (i) probe the domain structure of the alloy phases, and (ii) obtain their accurate compositions. We performed high-resolution mapping of the elemental composition on the single crystals of the alloys (Fig. 3c–e) as well as on the microparticles obtained by dispersing the single crystals of the alloys in ethanol (Fig. S19†). Fig. 3c–e show that the alloy crystals show homogenous distribution of molecular components within the resolution of the EDX mapping (2 nm). Since the domain structure from the EDX spectra implies the molecular level mixing of different components in the alloy crystal lattices, such a homogenous distribution can lead to new type of intermolecular interactions – different from those present in the parent crystals. For example, the nature of intermolecular interactions present in the Alq_3–Crq_3 alloy crystal could be different from those in Alq_3 and Crq_3 parent crystals. To probe any intermolecular effects such as charge transfer between the different components in the alloy crystals, we performed Raman spectroscopic studies. Fig. 4a–d shows the Raman spectra measured on the single crystals of pure Alq_3, Gaq_3, Crq_3, Inq_3 and their alloy crystals. In this study, we focused on the spectral range of 80–800 cm^{-1} which contain the characteristic peaks corresponding to the metal–ligand inter-actions. For pure Alq_3 crystals, we observe a peak at 118 cm^{-1} corresponding to the Al–oxine deformation and Al–N stretching, and a significant peak is observed at 525 cm^{-1} corresponding to ring deformation and Al–O stretching. The peak observed at 314 cm^{-1} is attributed to Al–N stretching and C–C–O bending.[31,32] All these peaks are characteristic features of the *mer* isomer of Alq_3 and it confirms that the crystals obtained are in *mer* form. All the observed peak positions and their vibrational assignments are tabulated in Tables S10 and S11 in the ESI.† Gaq_3 and Crq_3 crystals also showed similar peaks with slight differences in the peak positions with the change in the central metal atom. However, the spectra obtained for pure Inq_3 crystals are different from those of the Alq_3, Gaq_3 and Crq_3. A comparison of the Raman spectra obtained for Inq_3 with those reported in the literature for *fac*-Alq_3 indicate that the crystals could be predominantly in *fac* form[31] as it was also indicated by SCXRD measurements (since the weakly diffracting single crystals of Inq_3 were too small to obtain complete diffraction data for the structural refinement, only the unit cell parameters were obtained from the SCXRD measurements). Raman spectra of the binary alloy crystals formed by Alq_3, Gaq_3 and Crq_3 were found to be very similar to their parent crystals with no significant shifts in their characteristic peak positions.[31,32] This implies the absence of any considerable charge transfer type interactions between the molecular components in the alloys. An observable effect in the Raman spectra of the alloy crystals is a relative broadening of these characteristic peaks compared to parent crystals. The fact that the characteristic peaks corresponding to the M–O and M–N stretching modes do not show any significant change in the alloy crystals (compared to the parent crystals) further substantiates our argument that the bond distance averaging in the alloy structures is the consequence of the crystallographic spatial averaging rather that a bond relaxation effect. On the other hand, alloys formed by Inq_3 show a different trend from that of the pure Inq_3 crystals. As discussed earlier, the pure Alq_3 Raman spectrum corresponds to the *mer* isomeric form while that of Inq_3 exhibit spectral features corresponding to *fac* isomer as it is the preferred isomer for Inq_3. However, the Raman spectra of the alloy phases of Inq_3 reveal an intriguing trend: when the composition of Alq_3 is higher in Alq_3–Inq_3 alloy crystal, the spectra match well with that of the *mer* isomeric form. On the other hand, as the concentration of Alq_3 decreases, the

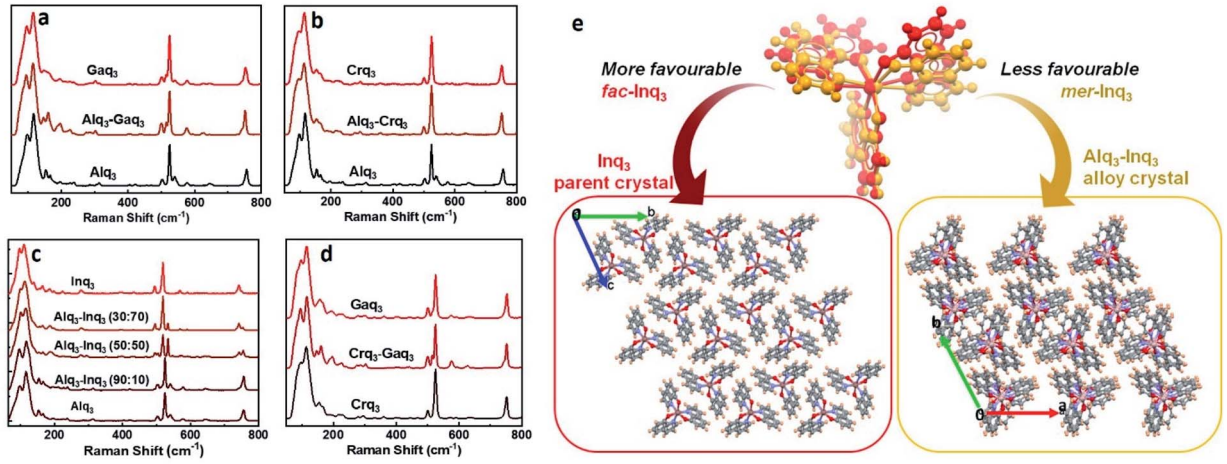

Fig. 4 (a–d) Raman spectra of Alq_3, Gaq_3, Crq_3, Inq_3 and their binary alloys measured on single crystals. (e) Structural overlay of *fac*-Inq_3 and *mer*-Inq_3 along with the crystal packing diagrams for *fac*-Inq_3 and the supramolecular 'entrapment' of *mer*-Inq_3 in the lattice of *mer*-Alq_3 leading to Alq_3-Inq_3 alloy crystals.

characteristic peaks of the *mer* isomer disappears and peaks corresponding to *fac* isomer emerge in the spectra (Fig. 4c). In crystals of Alq_3, the peak at 525 cm^{-1} corresponds to *mer* isomer and the peaks at 535 cm^{-1} and 548 cm^{-1} correspond to *fac* isomer. These peaks at 535 cm^{-1} and 548 cm^{-1} in Alq_3–Inq_3 alloy crystals with higher composition of Inq_3, such as Alq_3–Inq_3 (50 : 50), and Alq_3–Inq_3 (30 : 70) are replaced by a new peak at 525 cm^{-1} for alloy crystals with low composition of Inq_3 (as in 90 : 10 alloy of Alq_3–Inq_3). This implies that the relatively less stable *mer*-isomer of Inq_3 could be getting entrapped in the Alq_3–Inq_3 alloy crystal lattice, where it is a minor component.

Optical bandgaps of the alloys from UV-Vis diffuse reflectance spectra

A major consequence of the mixing of different molecules that are chemical analogues in the alloy phases could be the possible mixing of their electronic states. This could manifest as changes in the energy band gaps of the alloy crystals. In a recent report, we demonstrated that alloy formation can indeed lead to tuning in optical band gaps of crystals (even in the absence of π–π stacking) in the crystal structure.[17] The bandgap is a fundamental feature of a material that is linked to many of its optical and electronic properties. Especially since the Mq_3 series of compounds are OLED emissive layer materials, the trends in variation of band gaps in the alloy crystals is of particular interest. Hence, we measured UV-visible diffuse reflectance spectra on the solid-state samples of pure Mq_3 crystals and their binary alloys. The diffuse reflectance spectra were transformed using the Kubelka–Munk function[33] and the optical bandgaps were estimated from Tauc's plots.[34] The bandgaps observed for the series of pure crystals are in the following order Crq_3 < Gaq_3 < Alq_3 < Inq_3. Fig. S12† shows that Tauc's plot of Crq_3 shows a distinct feature of two separate slopes. It should be noted that the Tauc plot is usually effective when there is nearly zero absorption below the band gap energy, however in case of Crq_3 and its alloy crystals, there is a fair amount of absorption below the band gap energy. These absorption features usually arise from impurity or modified structure, or surface modifications. Hence a modified Tauc plot is used in these cases.[35] See ESI Fig. S10–S14† for Tauc's plots of all the Mq_3 crystals and their alloys. The values of the optical bandgaps for the parent crystals and their alloys are given in Table 1. Notably for Alq_3–Gaq_3 alloys the bandgap was found to be intermediate to those of pure Alq_3 and Gaq_3 similar to the trend we reported recently for diphenyl dichalcogenide alloys.[17] In case of Alq_3–Inq_3 alloys the tuning of bandgap to intermediate values (of Alq_3 and Inq_3) is observed for lower composition of Alq_3. Higher concentration of Alq_3 (lower concentration of Inq_3) in the alloy phase leads to a significant lowering of the band gap compared to the values of both pure Inq_3 and Alq_3. A similar trend is also observed for Gaq_3–Inq_3 alloy phases for which bandgap tuning (at high compositions of Inq_3) and bandgap lowering (at low compositions of Inq_3) were observed.

Table 1 Optical bandgaps (eV) for the crystalline Mq_3 samples and their binary alloys obtained from UV-vis diffuse reflectance spectra

	Composition ratios				
Alloy	100 : 0	90 : 10	50 : 50	30 : 70	0 : 100
Alq_3–Gaq_3	2.65	2.63	2.62	2.60	2.59
Alq_3–Inq_3	2.65	2.61	2.67	2.66	2.71
Gaq_3–Inq_3	2.59	2.55	2.6		2.71
Alq_3–Crq_3	2.65	2.54	2.53		2.53
Gaq_3–Crq_3	2.59	2.53	2.53		2.53

A conjoined analysis of the features from Raman spectra alongside SCXRD structures suggest that the possible origin of this distinct trend in bandgaps is in the preferential stabilization of different stereoisomers of Inq_3 with different compositions in its alloys. We find that the supramolecular entrapment of *mer*-Inq_3 (an otherwise unfavored isomer of Inq_3) as a minor component in the lattice of a *mer*-Alq_3 or *mer*-Gaq_3 major component could be the structural origin of this trend. This leads to intriguing effects in the emission properties of such alloy crystals as evident from the photoluminescence emission maxima described in the following section. Interestingly the bandgaps of the Alq_3–Crq_3 and Gaq_3–Crq_3 alloy crystals were found to be very close to the value of pure Crq_3 crystals (2.53 eV). Such a lowering of bandgap close to that of the paramagnetic component in molecular alloy crystals is hitherto unknown.

Effect of alloy formation on the photoluminescence emission

To probe the effect of alloy formation in the emission properties of the alloy crystals, we examined the photoluminescence (PL) on the single crystals of the pure Mq_3 and their binary alloys. The crystals mounted on a quartz plate were excited at a wavelength of 370 nm. The PL properties of pure Mq_3 systems are well studied and their emission is understood to originate from π–π* electronic transition in the ligand (from the HOMO localized around the phenoxide ring to the LUMO localized around the pyridyl ring).[36] Their emission maxima are known to vary with the central metal atom, polymorphic forms, and stereoisomers of the Mq_3. It was previously reported that with the increase in the size of the metal atom, there could be an increase in the covalent nature of the metal ligand bond leading to the red shift in the emission peak value.[20,37] Moreover, the *mer* isomeric forms showed a red shifted emission compared to the *fac* isomer in all the Mq_3 systems.[38] In addition to the stereochemical differences in the *mer* and *fac* isomers, variations in their crystal packing and intermolecular interactions might also be resulting in different relative energies for the ground and excited states – leading to shifts in their corresponding emission wavelengths. We observed the following trend in the wavelengths of emission maxima (λ_{max}) for the series of crystals studied here (Fig. 5): Gaq_3 (526 nm) > Alq_3 (504 nm) > Inq_3 (495 nm). Notably in the case of Crq_3 no photoluminescence emission was observed. This is evident from the optical microscopic images of Crq_3 single crystals (Fig. 5a) as well from the fluorescence spectra (Fig. 5d). Although the PL emission maximum of Inq_3 (at 498 nm) seems to defy the trend with respect to metal atom size, it is to be noted that the crystal form of Inq_3 obtained in this study are found to be *fac* form (the

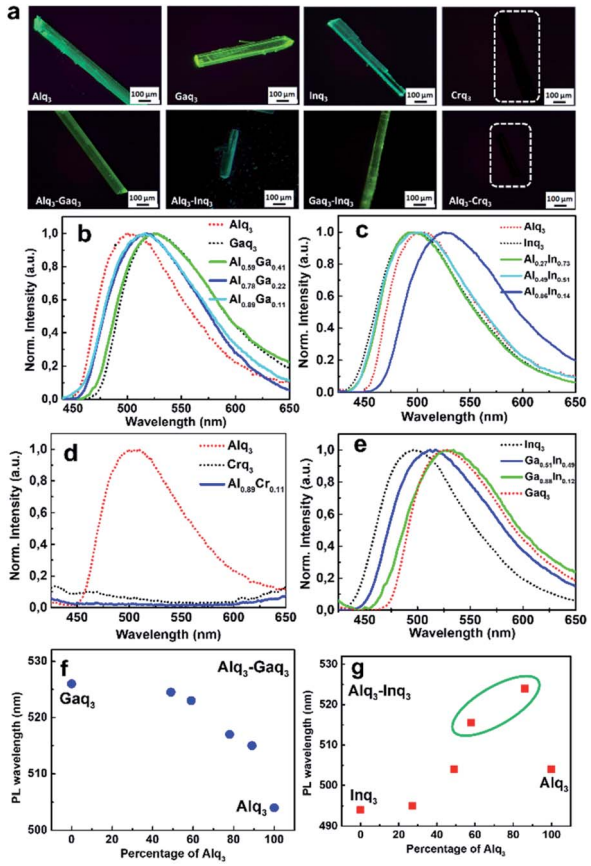

Fig. 5 (a) Optical microscopic images of the single crystals of the parent compounds (top row) and some binary alloys (bottom row), under UV light (λ = 395 nm). (b–e) Photo-luminescence spectra of Alq_3, Gaq_3, Inq_3 and Crq_3 in comparison with those of the binary alloys (background corrected). The absence of PL in Crq_3 and quenching of PL in Alq_3–Crq_3 alloy are evident from (d). The samples are excited at λ = 370 nm. (f) The tuning in λ_{max} of the PL emission in Alq_3–Gaq_3 alloy crystals, and (g) the red shifts in the λ_{max} in Alq_3–Inq_3 alloy crystals away from the λ_{max} values of the parent crystals.

more stable stereoisomer for Inq_3). The emission maximum we obtained for Inq_3 matches with the previously reported PL spectra of *fac*-Inq_3 in powder form.[38] Further, we examined the emission features in the PL spectra of the binary alloy crystals. In the case of Alq_3–Gaq_3 alloy crystal, we observed a tuning of the emission wavelength between the parent compounds *i.e.*, the emission maxima of the alloy crystals fall between the emission maxima of pure Alq_3 and Gaq_3 (Fig. 5b). With increasing concentration of Gaq_3 in the alloy, the emission showed a red shift. However, in the case of Alq_3–Inq_3 alloy crystals, the trend was quite different. In Alq_3–Inq_3 alloy crystals with higher composition of Alq_3, the emission peak exhibits a red shift compared to both the parent compounds, however, for lower compositions of Alq_3, the peak positions are close to the parent compounds (Fig. 5c and g, Table 2). The significant red shifts in the PL emission maxima of Alq_3–Inq_3 alloys red-shifted from those of the parent crystal forms may be understood in terms of the preferred stereoisomer and the lattice structure of Inq_3 molecules in their alloy phases. Possible explanations for the observed red shifts can be (i) charge transfer interaction between Inq_3–Alq_3 molecules in the crystal lattice leading to changes in the electronic energy levels, or (ii) supramolecular entrapment of the relatively less stable *mer* isomer of Inq_3 in the crystal lattice of the alloys. The latter is consistent with our structural and spectroscopic observations on the alloys. The crystal packing features of the major component lattice of the *mer*-ε Alq_3 prefers the incorporation of *mer*-Inq_3 compared to *fac*-Inq_3. Hence the possible origin of the red shifts observed in the PL emission should be the occurrence of the otherwise less stable *mer*-Inq_3 'trapped' in the alloys, which is supported by SCXRD and Raman spectral analysis as well as by the trend observed in the optical bandgaps.

Quenching of photoluminescence emission in the alloy crystals by the paramagnetic Crq_3 molecules

As mentioned above, the crystals of Crq_3 exhibit no significant PL emission (Fig. 5). However, we observed an intriguing phenomenon of fluorescence quenching caused by Crq_3 molecules in its alloy crystals. The binary alloys of Crq_3 with Alq_3 and Gaq_3 shows an effective quenching of PL emission. A similar phenomenon of quenching is also found for the ternary alloy crystals of $Al_xGa_yCr_{1-x-y}q_3$ and the quaternary alloy crystals of $Al_xGa_yIn_zCr_{1-x-y-z}q_3$. Crq_3 is paramagnetic, with the central Cr^{3+} atom having an electronic configuration of $3d^3$ ($t_{2g}^3e_g^0$). It is known that paramagnetic metal centers can interact with the excited states of fluorescing molecules leading to a quenching in fluorescence.[39,40] Fluorescence quenching by paramagnetic metal ions, such as Cr^{3+}, Fe^{3+}, Co^{2+}, Ni^{2+}, and Cu^{2+} have been reported,[41–43] and this phenomenon has been utilized in the detection of nitroxyl (HNO) in biological systems.[40] On the other hand, fluorescence enhancement induced by Cr^{3+} ions upon complexation with the ligand molecules is also reported.[43] It should be noted that most of this reported examples of

Table 2 Photoluminescence emission maxima (λ_{max} in nm) of the binary alloy crystals

Alq_3–Gaq_3		Alq_3–Inq_3		Gaq_3–Inq_3	
Composition	Em. λ_{max}	Composition	Em. λ_{max}	Composition	Em. λ_{max}
Gaq_3 pure	526	Inq_3 pure	495	Gaq_3 pure	526
$Al_{0.59}Ga_{0.41}$	523	$Al_{0.27}In_{0.73}$	496	$Ga_{0.88}In_{0.12}$	527
$Al_{0.78}Ga_{0.22}$	517	$Al_{0.49}In_{0.51}$	502	$Ga_{0.51}In_{0.49}$	515
$Al_{0.89}Ga_{0.11}$	515	$Al_{0.86}In_{0.14}$	524		
Alq_3 pure	504	Alq_3 pure	504	Inq_3 pure	495

fluorescence quenching or enhancement are associated with the complexation of paramagnetic metal ions with fluorophore molecules in solution state. The mechanism of quenching by paramagnetic metal centers are generally understood to be based on the photoinduced electron transfer (PET) from a singlet excited state of the fluorophore to paramagnetic metal center upon metal–ligand complexation. However, in the present study the fluorescence quenching is found to be originating from sheer intermolecular interactions between the Crq_3 molecules and the fluorescing molecule such as Alq_3 or Gaq_3 in the alloy lattice. Moreover, we find that the presence of Crq_3 leads to highly efficient fluorescence quenching in its molecular alloys with Alq_3 and Gaq_3 – not only in 1 : 1 alloys, but also in alloys with compositions as low as ~5% of Crq_3. These observations indicate a highly homogenous mixing of the molecular components in the alloy crystals, allowing effective interaction of the paramagnetic Crq_3 molecules with the electronic states of the Alq_3 or Gaq_3 molecules in the neighborhood of the alloy lattices. These results call for in-depth experimental and theoretical investigations, as the exact origin of the quenching phenomenon caused by the intermolecular interactions in the Crq_3 alloy crystals are not clear.

Conclusion

In summary, the molecular alloys formed by the Mq_3 series of compounds reported in this study exhibit intriguing trends with respect to their spectral and emission properties. The detailed analysis combining SCXRD, EDX and Raman spectra reveal correlations with the observed trends in their structure, optical band gaps and photoluminescence emission properties. In addition, we have reported the rare examples of ternary and quaternary molecular alloys formed by nonplanar molecules. The highly efficient fluorescence quenching caused by Crq_3 in its molecular alloy crystals reveals the effect of paramagnetic molecular components in the photoluminescence of alloy phases and provides further evidence for the highly homogenous nature of these alloys. The trends in PL emission peaks observed for different series of binary alloys have been corelated with the trends in their optical band gaps as well as Raman spectroscopic features and the stereoisomeric preference for *mer* or *fac* forms. We have shown that the formation of molecular alloys of Inq_3 with Alq_3 leads to a supramolecular entrapment of the less favored *mer* stereoisomer of Inq_3 in the alloy crystal lattice, leading to red shifts in the emission properties. Alloy crystal engineering using molecular components of chemical analogues as demonstrated in this study could be an efficient design strategy to fine tune the photophysical properties of functional molecular materials.

Data availability

The crystallographic information files have been deposited in the CCDC database with CCDC deposition numbers 2073957–2073962, 2074033–2074036, 2074042–2074044, 2074050–2074051, 2074080–2074081.

Author contribution

RT and SPT performed conceptualisation, data curation, formal analysis, investigation, methodology, and writing of the original draft. HL, AHM, MB and VB performed data curation, formal analysis and methodology. BBI performed conceptualisation, funding acquisition, project administration, supervision, discussion, review and editing.

Conflicts of interest

There are no conflicts to declare.

Acknowledgements

This work was supported by the Villum Foundation grant to BBI. VB acknowledges Novo Nordisk foundation (grant number NNF20OC0061417). SPT acknowledges EU funding for Marie Skłodowska-Curie Individual fellowship (grant number 798633). We thank Prof. Brian Julsgaard for useful discussions.

References

1 G. R. Desiraju, *J. Am. Chem. Soc.*, 2013, **135**, 9952–9967.
2 D. S. Reddy, D. C. Craig and G. R. Desiraju, *Chem. Commun.*, 1994, 1457–1458, DOI: 10.1039/C39940001457.
3 M. K. Mishra, U. Ramamurty and G. R. Desiraju, *J. Am. Chem. Soc.*, 2015, **137**, 1794–1797.
4 S. P. Thomas, R. Sathishkumar and T. N. Guru Row, *Chem. Commun.*, 2015, **51**, 14255–14258.
5 M. Lusi, *CrystEngComm*, 2018, **20**, 7042–7052.
6 S. Chakraborty, S. Joseph and G. R. Desiraju, *Angew. Chem., Int. Ed.*, 2018, **57**, 9279–9283.
7 M. Paul, S. Chakraborty and G. R. Desiraju, *J. Am. Chem. Soc.*, 2018, **140**, 2309–2315.
8 S. Chakraborty and G. R. Desiraju, *Cryst. Growth Des.*, 2018, **18**, 3607–3615.
9 M. Dabros, P. R. Emery and V. R. Thalladi, *Angew. Chem., Int. Ed.*, 2007, **46**, 4132–4135.
10 M. Lusi, *Cryst. Growth Des.*, 2018, **18**, 3704–3712.
11 X. Xu, B. Shan, S. Kalytchuk, M. Xie, S. Yang, D. Liu, S. V. Kershaw and Q. Miao, *Chem. Commun.*, 2014, **50**, 12828–12831.
12 M. Schwarze, W. Tress, B. Beyer, F. Gao, R. Scholz, C. Poelking, K. Ortstein, A. A. Günther, D. Kasemann, D. Andrienko and K. Leo, *Science*, 2016, **352**, 1446.
13 C. J. Adams, M. F. Haddow, M. Lusi and A. G. Orpen, *Proc. Natl. Acad. Sci. U.S.A.*, 2010, **107**, 16033.
14 W.-Q. Liao, D. Zhao, Y.-Y. Tang, Y. Zhang, P.-F. Li, P.-P. Shi, X.-G. Chen, Y.-M. You and R.-G. Xiong, *Science*, 2019, **363**, 1206.
15 R. A. Wiscons, V. Coropceanu and A. J. Matzger, *Chem. Mater.*, 2019, **31**, 6598–6604.
16 J.-H. Dou, Z.-A. Yu, J. Zhang, Y.-Q. Zheng, Z.-F. Yao, Z. Tu, X. Wang, S. Huang, C. Liu, J. Sun, Y. Yi, X. Cao, Y. Gao, J.-Y. Wang and J. Pei, *J. Am. Chem. Soc.*, 2019, **141**, 6561–6568.

17 S. P. Thomas, R. Thomas, T. B. E. Gronbech, M. Bondesgaard, A. H. Mamakhel, V. Birkedal and B. B. Iversen, *J. Phys. Chem. Lett.*, 2021, 3059–3065, DOI: 10.1021/acs.jpclett.1c00614.
18 X. Han, Y. Lei, Q. Liao and H. Fu, *Angew. Chem., Int. Ed. Engl.*, 2021, **60**, 3037–3046.
19 C. W. Tang and S. A. VanSlyke, *Appl. Phys. Lett.*, 1987, **51**, 913–915.
20 C. H. Chen and J. Shi, *Coord. Chem. Rev.*, 1998, **171**, 161–174.
21 V. A. Montes, R. Pohl, J. Shinar and P. Anzenbacher Jr, *Chem.–Eur J.*, 2006, **12**, 4523–4535.
22 J. P. Heiskanen and O. E. O. Hormi, *Tetrahedron*, 2009, **65**, 8244–8249.
23 C. Dai, Z. Wei, Z. Chen, X. Yan, J. Fan, Y. Yang, Z. Pang and S. Han, *ACS Appl. Energy Mater.*, 2018, **1**, 4367–4373.
24 M. Rajeswaran, T. N. Blanton, C. W. Tang, W. C. Lenhart, S. C. Switalski, D. J. Giesen, B. J. Antalek, T. D. Pawlik, D. Y. Kondakov, N. Zumbulyadis and R. H. Young, *Polyhedron*, 2009, **28**, 835–843.
25 R. Katakura and Y. Koide, *Inorg. Chem.*, 2006, **45**, 5730–5732.
26 C. F. R. A. C. Lima, R. J. S. Taveira, J. C. S. Costa, A. M. Fernandes, A. Melo, A. M. S. Silva and L. M. N. B. F. Santos, *Phys. Chem. Chem. Phys.*, 2016, **18**, 16555–16565.
27 Y. Lei, Y. Sun, Y. Zhang, H. Zhang, H. Zhang, Z. Meng, W.-Y. Wong, J. Yao and H. Fu, *Nat. Commun.*, 2018, **9**, 4358.
28 M. A. Spackman and D. Jayatilaka, *CrystEngComm*, 2009, **11**, 19–32.
29 M. J. Turner, S. P. Thomas, M. W. Shi, D. Jayatilaka and M. A. Spackman, *Chem. Commun.*, 2015, **51**, 3735–3738.
30 M. Brinkmann, B. Fite, S. Pratontep and C. Chaumont, *Chem. Mater.*, 2004, **16**, 4627–4633.
31 S.-Y. Hung, R.-L. Kao, K.-Y. Lin, C.-C. Yang, K.-S. Lin, Y.-C. Chao, J.-S. Wang, J.-L. Shen and K.-C. Chiu, *Mater. Chem. Phys.*, 2015, **154**, 100–106.
32 M. Halls and R. Aroca, *Can. J. Chem.*, 1998, **76**, 1730–1736.
33 J. H. Nobbs, *Rev. Prog. Coloration Relat. Top.*, 1985, **15**, 66–75.
34 J. Tauc, *Mater. Res. Bull.*, 1968, **3**, 37–46.
35 P. Makuła, M. Pacia and W. Macyk, *J. Phys. Chem. Lett.*, 2018, **9**, 6814–6817.
36 J. G. Mahakhode, S. J. Dhoble, C. P. Joshi and S. V. Moharil, *Bull. Mater. Sci.*, 2011, **34**, 1649–1651.
37 B. J. Chen, X. W. Sun and Y. K. Li, *Appl. Phys. Lett.*, 2003, **82**, 3017–3019.
38 R. I. Avetisov, A. A. Akkuzina, A. G. Cherednichenko, A. V. Khomyakov and I. C. Avetissov, *Dokl. Chem.*, 2014, **454**, 6–8.
39 A. R. Freitas, M. Silva, M. L. Ramos, L. L. G. Justino, S. M. Fonseca, M. M. Barsan, C. M. A. Brett, M. R. Silva and H. D. Burrows, *Dalton Trans.*, 2015, **44**, 11491–11503.
40 W. Yang, X. Chen, H. Su, W. Fang and Y. Zhang, *Chem. Commun.*, 2015, **51**, 9616–9619.
41 A. W. Varnes, R. B. Dodson and E. L. Wehry, *J. Am. Chem. Soc.*, 1972, **94**, 946–950.
42 H. S. Jung, P. S. Kwon, J. W. Lee, J. I. Kim, C. S. Hong, J. W. Kim, S. Yan, J. Y. Lee, J. H. Lee, T. Joo and J. S. Kim, *J. Am. Chem. Soc.*, 2009, **131**, 2008–2012.
43 S. Pal, N. Chatterjee and P. K. Bharadwaj, *RSC Adv.*, 2014, **4**, 26585–26620.